Environ Sci Pollut Res (2016) 23:16164–16175
DOI 10.1007/s11356-016-6769-z

RESEARCH ARTICLE

Agro-industrial waste: a low cost adsorbent for effective removal of 4-chloro-2-methylphenoxyacetic acid herbicide in batch and packed bed modes

Sunil K. Deokar[1] · **Sachin A. Mandavgane**[1] · **Bhaskar D. Kulkarni**[2]

Received: 11 February 2016 / Accepted: 26 April 2016 / Published online: 6 May 2016

Abstract The present work describes the aqueous phase removal of 4-chloro-2-methylphenoxyacetic acid herbicide by rice husk ash (RHA) using batch and packed bed adsorption techniques. The effects of dosage, initial concentration, time, pH, temperature, and particle size of adsorbent in batch compared with effects of influent concentration, flow rate, and bed height in packed bed were studied. The particle size effect reveals that the removal is dependent on chemical composition (silica and carbon content) together with BET surface area of RHA. The aptness of Langmuir isotherm to batch data indicates the favorable adsorption whereas that of Temkin isotherm informs the heterogeneous nature of RHA. The kinetics of adsorption follows the pseudo-second order and Elovich models while thermodynamics of process indicates the exothermic adsorption. Among the models applied in packed bed study, the deactivation kinetic, Yoon–Nelson and bed depth service time (BDST) models are suitable to explain the packed bed adsorption. The adsorption capacity of RHA in packed bed study is found greater than that in batch. The adsorption capacity of RHA determined by the BDST model is 3019 mg/L for 90 % saturation of bed. The adsorption capacity of RHA based on weight is ~2.3 times and that based on surface area is ~55.55 times greater than that of granular activated carbon.

Keywords Rice husk ash · MCPA · Adsorption · Silica to carbon ratio · Packed bed model · Particle size

Responsible editor: Angeles Blanco

Electronic supplementary material The online version of this article (doi:10.1007/s11356-016-6769-z) contains supplementary material, which is available to authorized users.

✉ Sachin A. Mandavgane
mandavgane1@gmail.com

[1] Chemical Engineering Department, Visvesvaraya National Institute of Technology, South Ambazari Road, Nagpur 440010, India

[2] CSIR-National Chemical Laboratory, Dr. Homi Bhabha Road, Pune 411008, India

Introduction

4-Chloro-2-methylphenoxyacetic acid (MCPA) is a chlorophenoxy herbicide used as pre- and post-emergent to control the growth of weeds in a variety of crops such as grain, corn, sugarcane, and rice (Cabrera et al. 2011). MCPA is preferred due to its low cost, good selectivity, and compatibility with other herbicides (Marczewska et al. 2010). Being an anionic, MCPA is weakly retained by the components of soil sediment; it remains in dissolved form in soil solution (Cardoso et al. 2006). Its leaching occurs rapidly, leading to subsequent contamination of groundwater and surface water where it remains for several weeks (Marczewska et al. 2010). This influences the ecosystems and the quality of water resources. MCPA is a member of phenoxy acid herbicides which are declared as possible carcinogens and mutagens by the International Agency for Research on Cancer (IARC 1983).

Among the methods described in literature for pesticide removal, adsorption is an extensively implemented technique owing to its inherent advantages such as low cost, easiness in operation, simplicity of design, and insensitivity to toxic pollutants (Deokar and Mandavgane 2015a). Additionally, adsorption removes most of the pollutants rather than a specific kind (Singh 2009). MCPA adsorption only in batch is previously reported using several adsorbents such as activated carbons (Marczewska et al. 2010; Cho et al. 2006; Pérez et al. 2012; Gimeno et al. 2003; Ignatowicz et al. 2009), mineral

(Iglesias et al. 2010), layered double hydroxides (LDH) (Cardoso et al. 2006; Inacio et al. 2001; Bruna et al. 2009), soils (Cabrera et al. 2011; Hiller et al. 2012), organic polymer resin (Vergili et al. 2009), and spent bleaching earth (Mahramanlioglu et al. 2003). Based on the literature reviewed, the agrobased industrial wastes particularly the biomass ashes have not been used for the removal of pesticides such as MCPA.

One of the biomass ashes is rice husk ash (RHA) which is generated as waste after combustion of husk in rice mill/power plant. Based on the rice production in 2014 (FAO), the global generation of RHA was ~41 million tons, with ~9 million tons from India alone (Deokar et al. 2016). RHA thus produced in huge quantity should be utilized to minimize the disposal problem. Researchers have used RHA as an efficient adsorbent for removal of heavy metals, dyes, and phenols from water (Ahmaruzzaman and Gupta 2011). The chemical composition (silica, carbon, and metal oxides) and availability make RHA as an efficient and economical adsorbent. Though RHA is extensively employed as adsorbent, its utilization for pesticide adsorption has not been explored in detail. Therefore, RHA was selected in the current study to adsorb MCPA from aqueous phase.

According to the author's knowledge, the adsorption efficacy of previously employed adsorbents for MCPA removal is evaluated only for batch adsorption. But adsorption in packed column is commercially worthwhile because the continuous contact between adsorbate and adsorbent allows for efficient utilization of the adsorbent, thereby enhancing the treatment of the effluent. The objective of the study was to (i) investigate the adsorption potential of RHA in batch and packed bed removal of MCPA and to (ii) study the effect of chemical composition (i.e., silica and carbon content) of RHA on adsorption. To achieve these objectives, the adsorption isotherms and kinetics of the batch study have been examined for different experimental conditions. The packed bed data obtained for different concentrations, flow rates, and bed heights were analyzed using the deactivation kinetic model together with conventional packed bed models.

Materials and methods

Adsorbent

RHA supplied by M/s Yash Agro Ltd., Nagpur (India), was firstly screened using BS sieves, and the particle size less than 0.500 mm was used for adsorption study. The moisture, ash, volatile matter, and fixed carbon content of RHA were determined using standard method (IS 1350, 1984) of proximate analysis. The surface properties such as BET surface area, pore volume, and pore diameter were measured using Brunauer–Emmett–Teller (BET) method (Micromeritics, ASAP 2010, USA). The chemical composition of RHA was determined using XRF analyzer (PANalytical, PW 2403, Netherlands) and elemental analyzer (Elementar, vario Micro Cube, Germany). The functional groups on the RHA surface before and after adsorption were observed by Fourier transform infrared (FTIR) spectroscopy (Shimadzu, IR-Affinity-1, Japan).

Adsorbate

Analytical grade MCPA was purchased from Sigma-Aldrich, India, and a stock solution was prepared in ultrapure water. The molecular structure and properties of MCPA are given in ESM 1: Table 1S (Supplementary Information).

Experimental methods

Batch adsorption study

In batch experiments, the glass vials containing MCPA solution (20 mL, pH 3.7) and RHA were agitated at constant temperature in a water bath shaker for 12 h. The samples were filtered then centrifuged, and concentration of the supernatant was measured on a UV/vis spectrophotometer (Shimadzu, Model UV 1800, Japan) at 279 nm (λ_{max}). The average values of triplicate experiments were used in calculations. The percentage removal and adsorption capacity at any time (q_t, mg/g) and at equilibrium (q_e, mg/g) was calculated from initial and equilibrium concentrations (C_0, Ce, mg/L). The effects of parameters such as adsorbent dosage, initial concentration, temperature, contact time, solution pH, and particle size of adsorbent were studied. The solution pH, changed between 2 and 12, was measured using a pH meter (Eutech, Model 2700, India).

Packed bed adsorption study

A glass column (30 cm height, 1.2 cm internal diameter) with four alternative openings at different positions from the bottom was fabricated for packed bed removal of MCPA. As per requirement of bed height, RHA (g) was packed between two supporting layers of glass wool. An intention of using the glass wool was to prevent the loss of adsorbent. The column was then soaked by pumping deionized water using a peristaltic pump (Electro Lab, PP201V, India), so that the entrapped air was withdrawn through the bed. The actual experiments were started after keeping the column ideal for 12 h. The influent solution was forced in an upward direction, and effluent was collected intermittently from the outlet to measure the concentration. The constant influent rate of MCPA solution was maintained by a mounting rotameter between the pump and the column. The column experiments were performed for different influent concentration (C_0, mg/L), flow rate (Q, mL/

min), and bed height (Z, cm) at constant temperature (30 ±2 °C) and pH (3.7). The breakthrough (BT) curve (C_t/C_0 versus time) was plotted for each experiment. The breakthrough (t_b) point and saturation (t_s) point were considered at $C_t/C_0 = 0.10$ and $C_t/C_0 = 0.97$, respectively. The saturation capacity q_s (mg/g) and breakthrough capacity q_b (mg/g) of the column were calculated using Eqs. (1) and (2), respectively.

$$q_s = \frac{C_0 Q}{m} \int_0^{t_s} \left(1 - \frac{C_t}{C_0}\right) dt \quad (1)$$

$$q_b = \frac{C_0 Q}{m} \int_0^{t_b} \left(1 - \frac{C_t}{C_0}\right) dt \quad (2)$$

where m (g) is the mass of the adsorbent. The length of mass transfer zone (MTZ) necessary to determine the fraction of bed utilization (FBU) is calculated using Eq. (3).

$$MTZ = Z\left(1 - \frac{q_b}{q_s}\right) \quad (3)$$

Results and discussion

Characterization of RHA

The proximate analysis revealed that RHA contained 1.80 % moisture, 6.16 % volatile matter, 89.87 % ash, and 2.14 % fixed carbon. The carbon content determined by CHNS analysis was found to be 5.85 % whereas silica by XRF analysis was 81.78 %. Additionally, XRF analysis indicated the presence of metal oxides such as 4.08 % Al_2O_3, 1.87 % K_2O, 1.27 % Fe_2O_3, 1.27 % CaO, 0.78 % P_2O_5, 0.50 % MgO, 0.19 % Na_2O, and 0.12 % MnO in RHA. These metal oxides in contact with water develop the surface charges depending on the pH of the solution (Deokar et al. 2015b). This enables faster adsorption of ionic adsorbate due to electrostatic attraction. The single point area and BET surface area of RHA were measured to be 33.61 and 33.99 m^2/g, respectively. The micropore area of RHA was 5.67 m^2/g, whereas the external surface area was calculated as 28.32 m^2/g from BET surface and micropore areas. The Barrett–Joyner–Halenda (BJH) adsorption and desorption surface areas of RHA were 26.29 and 36.87 m^2/g, respectively. The single point total pore volume of pores (<20 Å) was 2.69×10^{-3} cm^3/g, while the cumulative pore volume of pores (17 Å < d < 3000 Å) was 5.30×10^{-2} cm^3/g. The BJH adsorption and desorption average pore diameters were 81 and 57 Å, respectively.

The FTIR spectra of MCPA (Fig. 1, spectrum a) show a peak at 1728 cm^{-1} indicating the presence of –C=O bonding

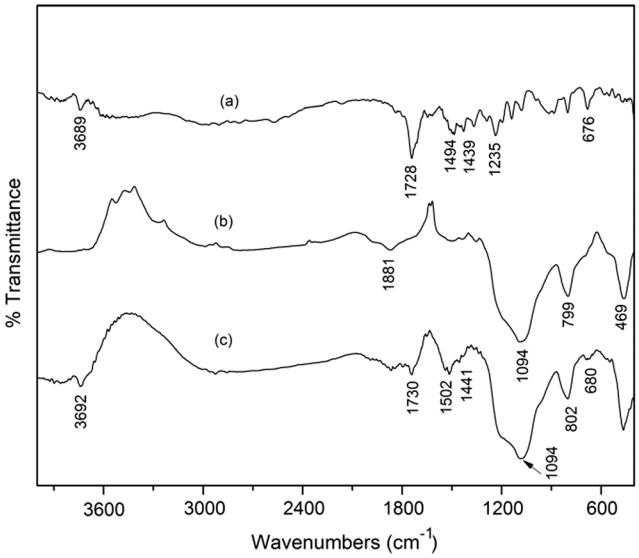

Fig. 1 FTIR spectra of **a** MCPA, **b** blank RHA, and **c** RHA after adsorption

in the carboxyl group (Bruna et al. 2009). The O–H deformation coupled with C–O stretching is showed by a band at 1235 cm^{-1} (Pavlovic et al. 2005). The O–H stretching band is presented by a weak peak at 3689 cm^{-1}. In addition, the peaks at 1439 and 1494 cm^{-1} in the MCPA spectrum correspond to CH_2 bending vibrations of alkanes and C=C vibrations of the aromatic ring, respectively. Moreover, a peak at 676 cm^{-1} indicates the C–Cl stretching vibration (Arivazhagan et al. 2011). The FTIR spectrum of blank RHA (i.e., before adsorption) presented in Fig. 1 (spectrum b) indicates the weak combinations and overtone absorption in the region at 1667 to 2000 cm^{-1}. The peaks in this region are assigned to monosubstitution to hexasubstitution of the aromatic ring (Pavia et al. 2008). The peaks at 1094 and 799 cm^{-1} in the RHA spectrum represent the stretching vibrations of Si–O–Si and H–C bonds, respectively, while the peak at 469 cm^{-1} is assigned for the Si–H bond (Deokar et al. 2016).

The RHA spectrum after adsorption of MCPA (Fig. 1, spectrum c) shows the appearance of a new peaks as well as shifting of some existing peaks. The appearance of the new peak at 1502 cm^{-1} is attributed to asymmetric COO^- stretching vibration ($\upsilon_{asym}COO^-$) of the carboxyl functional group (Kim and Hyun 2014). This indicates the attachment of anionic MCPA with positive metal oxides through electrostatic interaction (Kim and Hyun 2014). The spectrum showed the existence of peaks at 1730 and 1441 cm^{-1} which may be due to –C=O stretching and CH_2 bending, respectively, of the MCPA molecule adsorbed through the van der Waal force of attraction (Hermosin and Cornejo 1993). The shifting of a peak from 676 to 680 cm^{-1} is due to electron-donating electrostatic interaction of positive RHA surface with MCPA molecules.

Batch adsorption

Effect of RHA dosage

The change in removal of MCPA with RHA dosage was examined for 100 mg/L initial concentration by varying the dosage in a range of 0.25–3.5 g/20 mL solution at constant temperature (303 K), contact time (720 min), and pH (3.7). Results are plotted in ESM 1: Fig. 1S (Supplementary Information) which indicate the improvement in percentage removal with increase in RHA dosage. This is attributed to an increase in surface area with increase in dosage of RHA since surface area is a function of adsorbent dosage. The removal of MCPA was increased from 89 to 95 % for 2.5 to 3.5 g of RHA. The significant improvement in removal is not observed for higher dosages due to the establishment of equilibrium between solid-phase and liquid-phase MCPA molecules (Dutta et al. 2014; Srivastava et al. 2006). Therefore, 2.5 g/20 mL is selected as the optimum dosage for further studies in this work.

Effect of initial concentration and temperature

The initial concentration of MCPA was varied between 50 and 400 mg/L at a fixed contact time and pH. The experiments were performed at three different temperatures, viz., 303, 318, and 328 K, to examine the effect of temperature on adsorption of MCPA. The results in Fig. 2 express the reduction in percentage removal with increase in initial concentration. Since RHA has a finite number of adsorption sites, the removal is notably decreased at higher concentrations (Nawaz et al. 2014). However, it is observed that the amount (mg/g) of MCPA removed is increased with increase in concentration. This increase is due to equilibrium: a higher liquid concentration corresponds to a higher solid concentration at equilibrium. With increasing the temperature of the solution, uptake is decreased due to a reduction in the affinity of MCPA for RHA. This indicates the exothermic adsorption of MCPA on the RHA surface. This implies that the adsorption of MCPA on RHA may be physisorption because the exothermic adsorption is usually physisorption (Dutta et al. 2014).

Effect of contact time

The equilibrium time of MCPA adsorption on RHA was investigated by performing the experiments for different times at 100 mg/L, pH 3.7, and 303 K. It is evident from Fig. 3 that most of the MCPA is adsorbed within the first 10 min due to the fast rate of initial adsorption, after which the uptake rate gradually slows down resulting in system equilibration in approximately 120 min. Initially, the greater concentration gradient across the solid–liquid interface and available sites on the RHA surface may be mainly contributing to the high rate of adsorption which in turn reduced with increasing contact time (Dutta et al. 2014). The reduction of rate in the later part of adsorption may be due to aggregation of MCPA molecules within pores and saturation of the active site on the RHA surface, thereby increasing resistance for diffusion of molecules (Mane et al. 2007).

Effect of solution pH

The charge on surface of adsorbent and the degree of ionization of adsorbate depend on solution pH, therefore adsorption experiments were performed for different pH at fixed concentration (100 mg/L), time (720 min), and temperature (303 K). It can be observed in ESM 1: Fig. 2S (Supplementary Information) that the removal of MCPA reduced from 93 to 70 % when pH increased from 2 to 12. This is because of the

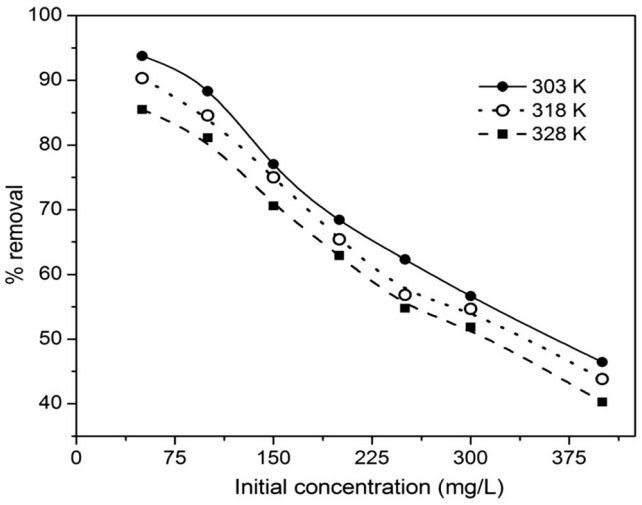

Fig. 2 Effect of initial concentration and temperature on removal of MCPA at 2.5 g RHA/20 mL

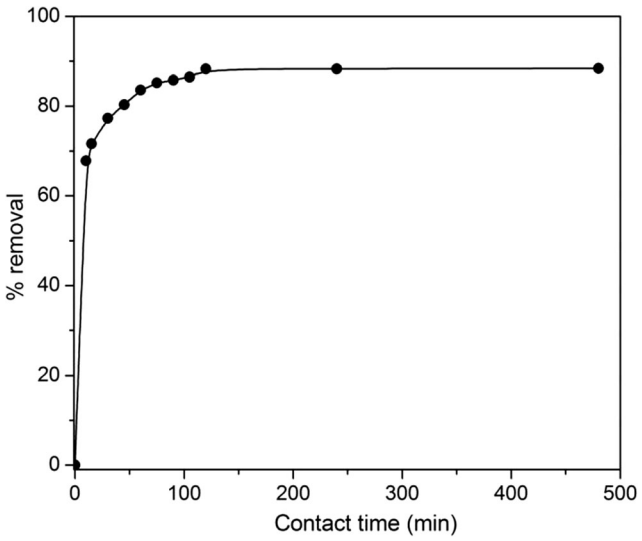

Fig. 3 Effect of contact time on removal of MCPA at 100 mg/L, pH 3.7, and 303 K

combined effect of point of zero charge (pHzpc) and solution pH on the charges developed on the RHA surface. pHzpc at which the adsorbent surface acts as neutral is reported to be 8.3 for RHA (Srivastava et al. 2006). At pH < pHzpc, the RHA surface is positively charged, and at pH > pHzpc, the reverse will occur. At pH <3.07 (i.e., pKa of MCPA), most of the MCPA is expected in molecular form and less in anionic form. Therefore, at lower pH, higher number of molecular MCPA due to van der Waals forces and lower number of anionic MCPA due to electrostatic attraction are adsorbed on the RHA surface. At higher pH, the anionic form of MCPA is greater in number than is the molecular form. The anionic MCPA is repelled by negative charges formed on the RHA surface at higher pH. Therefore, the removal is decreased with increase in solution pH.

Effect of particle size of RHA

The effect of particle size on adsorption of MCPA was investigated for five different particle size fractions of RHA at fixed concentration, time, and temperature. Results for particle size less than 0.089, 0.089–0.152, 0.152–0.251, 0.251–0.354, and 0.354–0.500 mm are presented in Fig. 4. It is observed that with increasing particle size of RHA, the percentage removal of MCPA is appreciably improved. It can be seen in Fig. 4 that the almost complete removal is achieved for the 0.354–0.500-mm particle size which is just around 40 % for particles less than 0.089 mm. To elucidate these results, the BET surface area and chemical composition (silica and carbon percentage) of the aforesaid particle size ranges are determined. The BET surface area and carbon percentage are enhanced whereas silica percentage is reduced with particle size (Fig. 4). Though the change in carbon percentage and silica percentage is small, the silica to carbon ratio is significantly decreased from 33 to 5

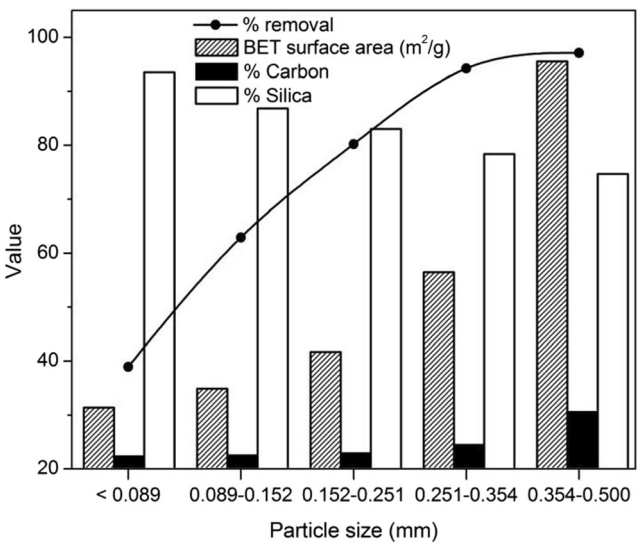

Fig. 4 Effect of particle size on removal of MCPA at 100 mg/L, 720 min, and 303 K

for the smallest to the largest particle size, respectively. The point of zero charge of silica is 2.2 and those of Fe_2O_3, Al_2O_3, and CaO are 6.7, 8.3, and 11, respectively. The silica forms a negative charge whereas metal oxides develop a positive charge on the surface when RHA is immersed in aqueous solution of pH ≈ 3.7 (Srivastava et al. 2008). Thus, MCPA being anionic is mostly adsorbed on carbon and metal oxides in RHA. Therefore, the higher BET surface area together with smaller silica to carbon ratio is responsible for the higher removal of MCPA on bigger particles than on smaller particles of RHA.

Isotherm modeling and thermodynamic properties

The most commonly applied isotherms, namely, Langmuir, Freundlich, and Temkin models (Jain et al. 2013), are considered in the present work to determine the adsorption capacity and adsorbent affinity. The non-linear forms of the Langmuir, Freundlich, and Temkin isotherm models are expressed by Eqs. (4), (5), and (6), respectively.

$$q_e = \frac{K_L q_{\max} C_e}{(1 + K_L C_e)} \tag{4}$$

$$q_e = K_F C_e^{1/n} \tag{5}$$

$$q_e = \frac{RT}{b_T} ln(A_T C_e) \tag{6}$$

where q_e (mg/g) and C_e (mg/L) are the capacity and concentration at equilibrium, respectively; q_{max} (mg/g) is the monolayer adsorption capacity. The Langmuir constant, denoted by K_L (L/g), is related to the affinity of binding sites. K_F [(mg/g)/(mg/L)$^{1/n}$] and n are the Freundlich constant and adsorption intensity factor, respectively. A_T (L/g) and b_T (J/mol) are Temkin constants related to binding at equilibrium and heat of adsorption, respectively. The isotherm parameters investigated at three different temperatures are presented in Table 1 for MCPA adsorption using RHA. The non-linear plots of isotherm models at temperature 303 K are presented in Fig. 5.

The values of coefficient of determination (R^2) in Table 1 are closer to 1 for Langmuir and Temkin isotherms than for Freundlich isotherm, which inform the aptness of Langmuir and Temkin models over the Freundlich model. The adsorption capacity (q_{max}) indicated by the Langmuir model is reduced with increment in temperature reflecting the exothermic adsorption. The reduction of affinity between MCPA and RHA is shown by decreasing values of constants, K_L for the Langmuir model and A_T for the Temkin model with increase in temperature. The dimensionless factor, [$R_L = 1/(1 + K_L C_0)$], for Langmuir isotherms was determined for 50–

Table 1 Isotherm parameters with coefficient of determination for MCPA adsorption on RHA at different temperatures

Isotherm models	Parameters	Temperature (K)		
		303	318	328
Langmuir	q_{max} (mg/g)	1.681	1.521	1.490
	K_L (L/g)	0.052	0.043	0.042
	R^2	0.991	0.991	0.991
Freundlich	n	3.13	2.90	2.68
	K_F [(mg/g)/(mg/L)$^{1/n}$]	0.288	0.237	0.226
	R^2	0.978	0.966	0.969
Temkin	A_T (L/g)	1.220	0.768	0.710
	b_T (kJ/mol)	6.615	7.128	7.501
	R^2	0.990	0.990	0.995

400-mg/L concentrations at three different temperatures and was found in between 0 and 1, indicating a favorable adsorption of MCPA on RHA in the temperature range of 303–328 K (Deokar and Mandavgane 2015b). The thermodynamic properties (Wu et al. 2013) such as change in enthalpy (ΔH), entropy (ΔS), and Gibbs free energy (ΔG) were calculated by using Eqs. (7) and (8).

$$\ln K_d = -\frac{\Delta H}{RT} + \frac{\Delta S}{R} \tag{7}$$

$$\Delta G = -RT\ln K_d \tag{8}$$

where K_d is an equilibrium distribution coefficient, and it is calculated as a ratio of equilibrium concentration of adsorbate in solid phase to liquid phase. R (8.314 J/mol K^{-1}) is the gas constant and T (K) is the absolute temperature. ΔH (–14.392 kJ/mol) and ΔS (–30.804 J/mol) were determined from the slope and intercept of the Van't Hoff plot ($\ln K_d$ versus 1/T), respectively. The negative value of ΔH stands for exothermic adsorption whereas the negative value of ΔS suggests the favorable adsorption with no structural change at the solid–liquid interface (Akhtar et al. 2007). ΔG values, found to be –5.096, –4.505, and –4.352 kJ/mol at 303, 318, and 328 K, respectively, are indicative of feasibility and spontaneity of adsorption.

Kinetic modeling

Adsorption kinetics elucidates the rate and detail mechanism of the adsorption process. In this study, the kinetics of MCPA adsorption is studied by applying the pseudo-first order (PFO), pseudo-second order (PSO), and Elovich (EL) models (Dutta et al. 2014). The plots of PFO (Eq. 9), PSO (Eq. 10), and EL (Eq. 11) models are given Fig. 6.

$$q_t = q_e\left(1-e^{-k_1 t}\right) \tag{9}$$

$$q_t = \frac{k_2 q_e^2 t}{1 + k_2 q_e t} \tag{10}$$

$$q_t = \frac{1}{\beta}\ \ln(\alpha\beta t) \tag{11}$$

where k_1 (min^{-1}), k_2 [g/(mg min)], and α [mg/(g min)] are rate constants; β (g/mg) is the desorption constant; and q_e is the equilibrium capacity. The coefficient of determination (R^2) was found to be 0.981 for PFO, 0.999 for PSO, and 0.994 for EL models which suggests the best fitting of PSO and EL models to the experimental data. The value of k_2 was calculated as 0.303 [g/(mg min^{-1})] whereas α and β was 31.14 [mg/(g min^{-1})] and 15.63 (g/mg), respectively. EL

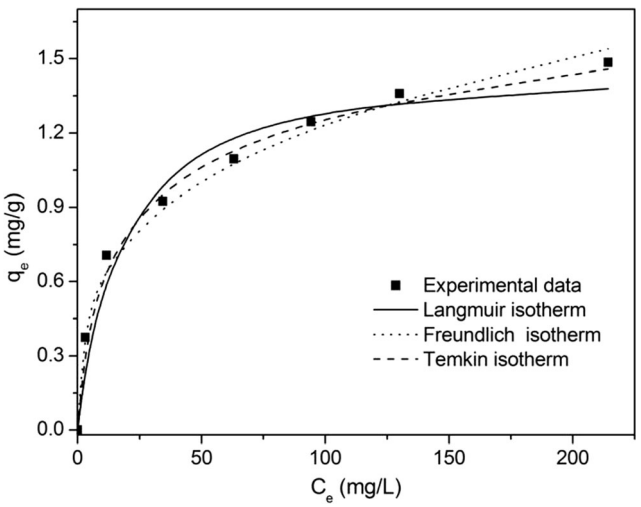

Fig. 5 Isotherm models for adsorption of MCPA on RHA at 303 K

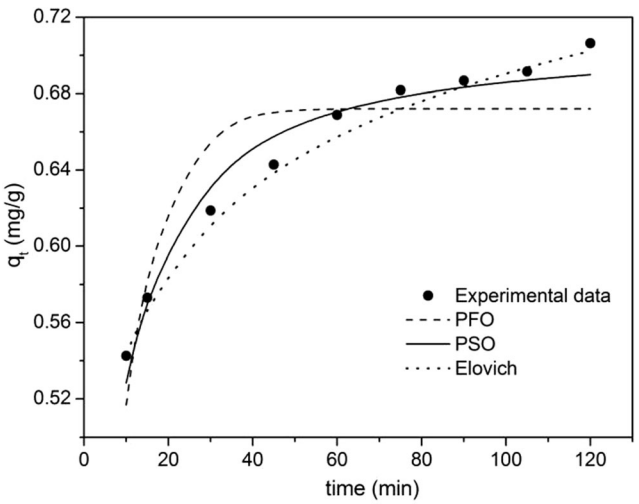

Fig. 6 Plots of kinetic models for adsorption of MCPA on RHA

model informs the heterogeneous surface of RHA indicating the presence of active sites with different energies.

Packed bed adsorption

Effect of influent concentration

The influent concentration was increased from 50 to 150 mg/L at constant Q (1 mL/min) and Z (9.5 cm) in packed bed adsorption. Results are plotted in the form of BT curves in ESM 1: Fig. 3S (Supplementary Information) which indicates the early saturation of the RHA bed for higher C_0. This is due to the limited adsorption sites for higher C_0. Consequently, the steeper BT curve is obtained at higher C_0 leading to a reduction in breakthrough and saturation times (ESM 1: Table 2S, Supplementary Information). Adsorption becomes difficult at higher C_0 as the saturation rate of the RHA bed increases with C_0. However, the bed capacities (q_b, q_s) in Table 2S are enhanced at higher C_0 due to the concentration gradient which offers greater driving force for mass transfer. The slow approach of the BT curve in the saturation stage of the column is attributed to the control of intraparticle diffusion over mass transfer (Srivastava et al. 2008). The MTZ (Table 2S) is expanded with C_0 due to higher increase in q_s than that of q_b at constant Z. The bed utilization is slightly decreased, but the percentage removal is notably reduced with C_0.

Effect of flow rate

The behavior of BT curves is studied by varying the flow rate (Q) between 1 and 3 mL/min at constant influent concentration (100 mg/L) and bed height (6.5 cm). It can be observed in Fig. 4S (ESM 1: Supplementary Information) that the extended BT curve is obtained for lower Q, resulting in higher t_s and q_s. With increase in Q, the reduction in capacity and percentage removal (Table 2S) are ascribed to the insufficient residence time of MCPA in the RHA bed. However, the length of MTZ is enhanced because of the increased mass transfer at higher Q. Sotelo et al. (2012) has earlier reported a similar behavior of MTZ in packed bed removal of pesticides using activated carbon. Both the percentage removal and FBU are inversely proportional to Q. It can be deduced from Table 2S that the performance of the RHA column is better at lower flow rate.

Effect of bed height

The BT curves in ESM 1: Fig. 5S (Supplementary Information) are obtained for different Z at fixed C_0 (100 mg/L) and Q (1 mL/min). With increase in bed height, the surface area of adsorbent is increased which leads to improvement in capacity as listed in Table 2S. The residence time of MCPA molecules in the RHA bed is longer for higher Z as the molecules have to pass through a longer length of the bed. Therefore, the column requires more time for saturation resulting in extended BT curve at higher Z. Because of higher q_b and q_s, the length of MTZ is significantly increased with Z. With expansion of MTZ with Z, the bed utilization is considerably improved, and therefore, the volume of MCPA solution treated is also increased. By contrast, the narrow MTZ for the lowest Z suggests efficient utilization of adsorbent, which would facilitate easy regeneration of adsorbent (Deokar and Mandavgane 2015a). However, q_b is less for lower Z due to axial dispersion, which controls the mass transfer mechanism (Sotelo et al. 2012). This indicates a shorter time for diffusion of MCPA molecules into RHA. Therefore, the beds of increased height may be recommended for better column performance.

Packed bed modeling

Bed depth service time model

The BDST model is based on surface reaction theory, and it assumes negligible intraparticle diffusion and resistance to external mass transfer. The BDST model given by Eq. (12) is applied to experimental data obtained for variable Z at constant C_0 and Q.

$$t = \frac{N_0}{C_0 U_0} Z - \frac{1}{C_0 K_{BD}} \ln\left(\frac{C_0}{C_t} - 1\right) \tag{12}$$

where U_0 (cm/min) is the linear flow velocity. The application of the BDST model at 10, 50, and 90 % BT of column is shown in Fig. 7. The sorption capacity, N_0 (mg/L), is calculated from the slope and is found to be

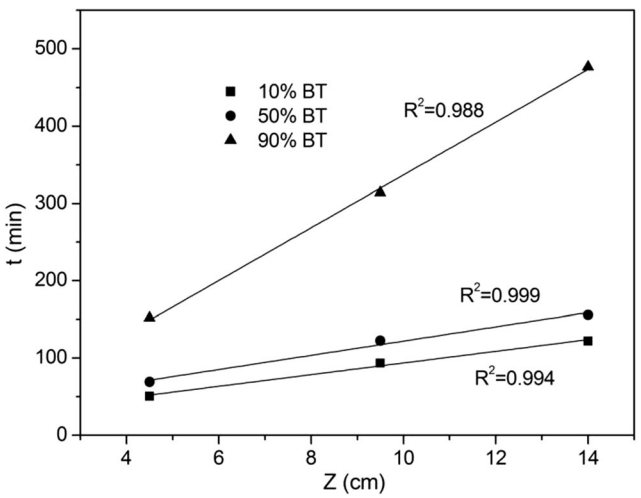

Fig. 7 BDST model for MCPA adsorption on RHA

668, 813, and 3019 for 10, 50, and 90 % BT, respectively. The rate constant, K_{BD} [L/(mg min^{-1})] determined from the intercept is 1.20×10^{-3} at 10 % and 4.98×10^{-3} at 90 % BT. The values of R^2 in Fig. 7 are slightly greater for 10 and 50 % BT than for 90 % BT. This may be due to intraparticle diffusion in the final stage of adsorption, leading to uneven variation in 90 % BT with change in Z. R^2 values close to 1 indicate the fitting of BDST at 10, 50, and 90 % BT of column. The 10 and 50 % BT lines are nearly parallel indicating a constant length of MTZ till 50 % saturation, after which MTZ is expanded due to intraparticle diffusion.

Application of the Bohart–Adams model

According to the Bohart–Adams model, the adsorption rate is proportional to the residual capacity of the adsorbent and the concentration of adsorbate (Han et al. 2009). This model was previously used to explain the behavior of the BT curve in the initial stage of adsorption (Han et al. 2009). Here, Eq. (13) shows the Bohart–Adams model applied when BT of the RHA column reaches 60 %. Comparison between experimental and predicted curves for this model is given in Fig. 8.

$$\ln\left(\frac{C_t}{C_0}\right) = K_{AB}C_0 t - K_{AB}N_0\left(\frac{Z}{U_0}\right) \tag{13}$$

The kinetic constant [K_{AB}, L/(mg min^{-1})] and sorption capacity (N_0, mg/L) are given in ESM 1: Table 3S (Supplementary Information). The sorption capacity (N_0) shown in Table 3S is directly proportional to C_0 and Z and inversely proportional to Q. The gradient at higher C_0 and surface area of RHA for higher Z are responsible for greater capacity. The lessening capacity with flow rate is due to the insufficient residence time for adsorption. The deviation between experimental and predicted values of (C_t/C_0) is calculated using Marquardt's percent standard deviation (MPSD), expressed in Eq. (14), and that between t_b values using percentage deviation Є, expressed in Eq. (15) (Srivastava et al. 2008). From the values of MPSD and Є in Table 3S, the good agreement between experimental and predicted results can be observed for few packed bed experiments.

$$MPSD = 100\sqrt{\frac{1}{N-P}\sum\left(\frac{\left(\frac{C_t}{C_0}\right)_{expt.} - \left(\frac{C_t}{C_0}\right)_{pred.}}{\left(\frac{C_t}{C_0}\right)_{expt.}}\right)^2} \tag{14}$$

$$\varepsilon = 100\left(\frac{t_{bexpt} - t_{bpred}}{t_{bexpt}}\right) \tag{15}$$

Application of Thomas model

The adsorbent capacity and BT curve are necessary for successful design of continuous adsorption process (Preetha and Viruthagiri 2007). These requirements can be accomplished by using the Thomas model. This model assumes second-order reversible reaction kinetics and the Langmuir isotherm; however, sorption is governed by not only chemical reaction kinetics but also interface mass transfer (Preetha and Viruthagiri 2007). This discrepancy may lead to some errors in certain conditions of packed bed adsorption. The Thomas model (Eq. 16) is applied to data in a range of $0.01 < (C_t/C_0) < 0.97$, and predicted BT curves (Fig. 9) are obtained.

$$\ln\left(\frac{C_0}{C_t} - 1\right) = \frac{K_T q_0 m}{Q} - K_T C_0 t \tag{16}$$

The adsorption capacity (q_0, mg/g) and kinetic constant [K_T, L/(mg min^{-1})] are listed in Table 3S. The capacity is enhanced with C_0 and Z whereas the kinetic constant is reduced with C_0 and Z. But the increment in Q shows reduction in capacity and growth in kinetic constant. A similar change in capacity and kinetic constant with change in C_0, Q, and Z was previously reported by (Aksu 2004). The deviation values in

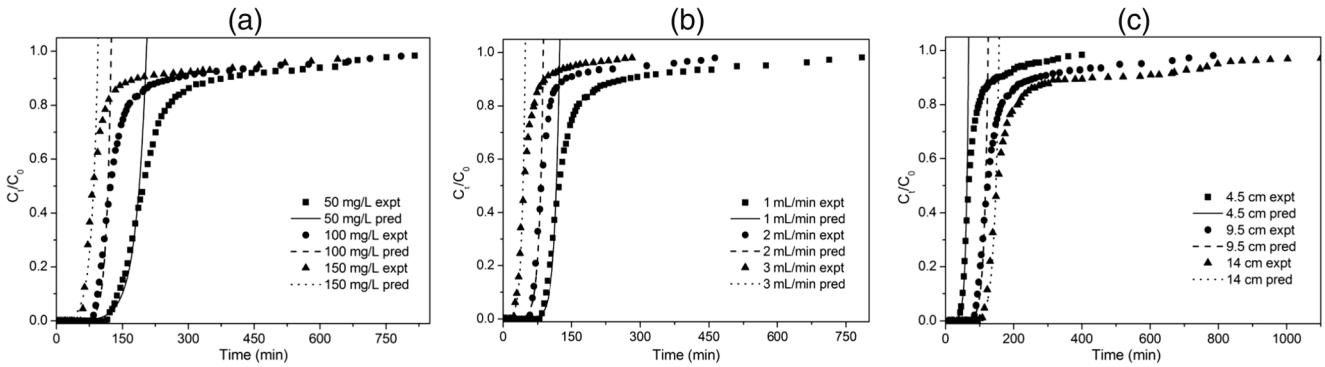

Fig. 8 Comparison between experimental and predicted breakthrough curves using Bohart–Adams model. **a** Q = 1 mL/min, Z = 9.5 cm; **b** C_0 = 100 mg/L, Z = 9.5 cm; **c** Q = 1 mL/min, C_0 = 100 mg/L

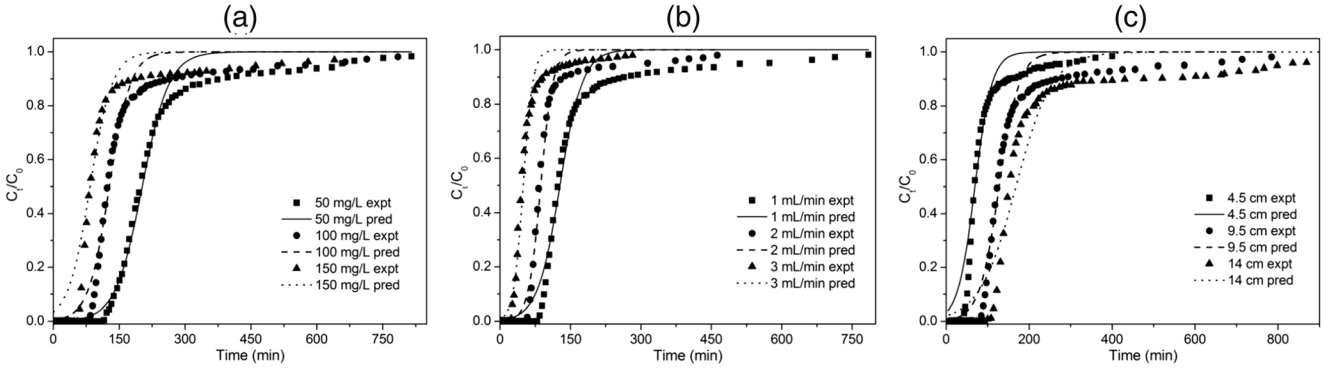

Fig. 9 Comparison between experimental and predicted breakthrough curves using Thomas model. **a** Q = 1 mL/min, Z = 9.5 cm; **b** C_0 = 100 mg/L, Z = 9.5 cm; **c** Q = 1 mL/min, C_0 = 100 mg/L

Table 3S indicate close approximation between experimental and predicted values for all experimental conditions although the greater deviations are evident at highest C_0, Q, and Z (expt. no. E4, E6, E9). The higher values of deviations may be due to the discrepancy which appeared while considering the assumptions in deriving the model.

Application of Yoon–Nelson model

The Yoon–Nelson model (Nethaji et al. 2013) (Eq. 17) is applied to experimental data for the $0.01 < (C_t/C_0) < 0.97$ range to predict the time necessary for 50 % saturation of the column. The Yoon–Nelson model is simpler and does not require any detailed data pertaining to adsorbate characteristics, adsorbent type, and physical properties of adsorbent bed (Deokar and Mandavgane 2015a).

$$\ln\left(\frac{C_t}{C_0 - C_t}\right) = K_{YN}t - t_{0.5}K_{YN} \tag{17}$$

where K_{YN} (min^{-1}) is the kinetic constant and $t_{0.5}$ (min) is the time necessary for 50 % saturation of the column. The kinetic constant, K_{YN}, in Table 3S is augmented due to driving force for mass transfer at higher C_0 and Q. At higher Z, MCPA molecules have to travel a longer path through the bed; therefore, the reduction of kinetic constant at higher Z is observed (Aziz et al. 2014). The BT curves predicted by the Yoon–Nelson model are compared with experimental BT curves in Fig. 10. Both the experimental and its predicted curves appear identical till $C_t/C_0 \approx 0.85$ for all experimental condition. The MPSD and Є values for Yoon–Nelson (Table 3S) are smaller than those for former packed bed models.

Application of deactivation kinetic model

The initial sorption rate and deactivation rate in case of gas–solid (packed bed) adsorption are usually determined by deactivation kinetic model (Hong et al. 2014). The model is based on isothermal, pseudo-steady-state conditions, negligible axial dispersion, and mass transfer resistance. In this model, single activity term is used to denote the effect of factors like pore structure, active surface area, and activity per unit area of adsorbent. In this study, Eq. (18) is applied for complete saturation of the RHA column and model parameters (Table 3S) are determined.

$$\frac{C_t}{C_0} = \exp\left[\frac{1-\exp(k_0 B[1-\exp(-k_d t)])}{1-\exp(-k_d t)}\exp(-k_d t)\right] \tag{18}$$

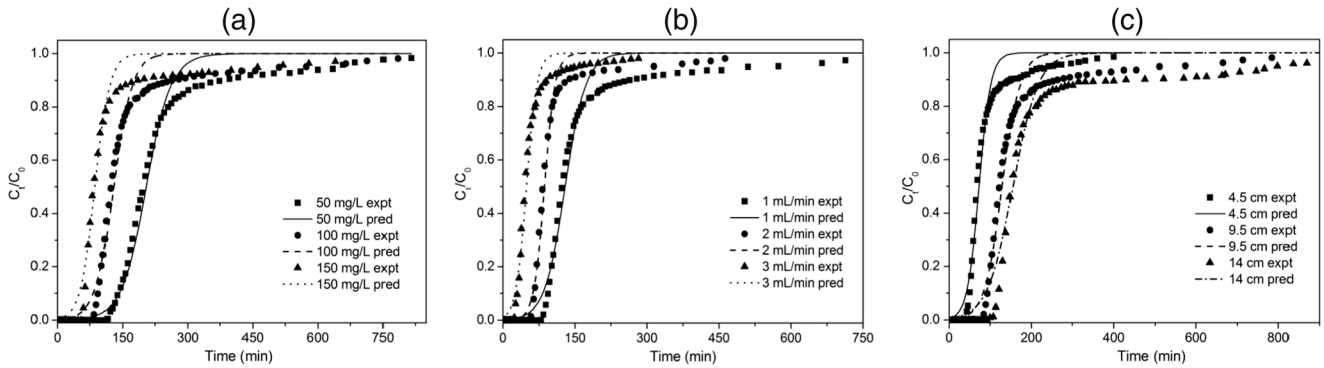

Fig. 10 Comparison between experimental and predicted breakthrough curves using Yoon–Nelson model. **a** Q = 1 mL/min, Z = 9.5 cm; **b** C_0 = 100 mg/L, Z = 9.5 cm; **c** Q = 1 mL/min, C_0 = 100 mg/L

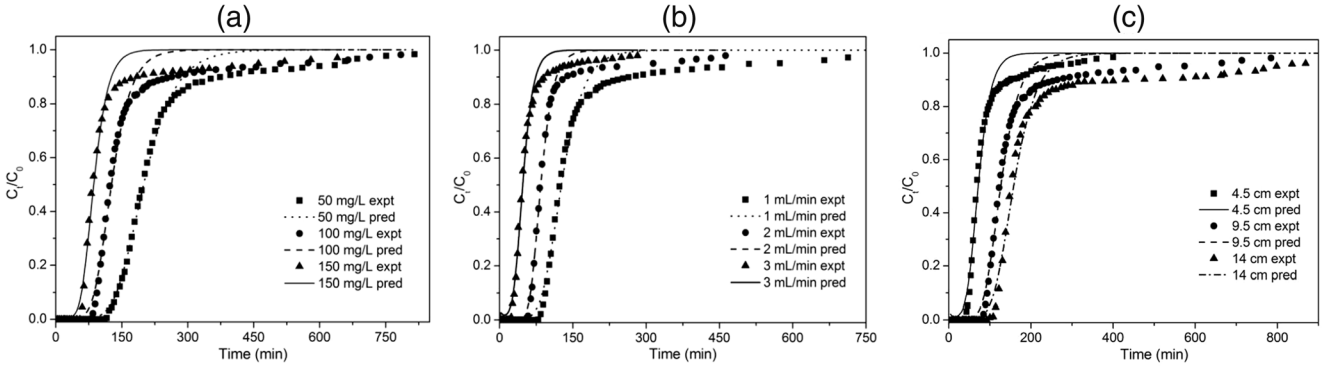

Fig. 11 Comparison between experimental and predicted breakthrough curves using deactivation kinetic model. **a** Q = 1 mL/min, Z = 9.5 cm; **b** C_0 = 100 mg/L, Z = 9.5 cm; **c** Q = 1 mL/min, C_0 = 100 mg/L

The initial sorption rate, k_0 [mL/(g min^{-1})] (Table 3S), is distinctly increased with Q whereas it is decreased with Z. The change in sorption rate is more significant for Q and Z than for C_0 due to simultaneous change in effluent concentration and weight–time factor (B = m/Q). It can be seen in Table 3S that the deactivation rate constant, k_d (min^{-1}), is higher for higher C_0 and Q at constant Z since the number of MCPA molecules adsorbed are higher on fixed number of adsorption sites. But deactivation constant is reduced due to increasing number of sites with increase in Z at constant C_0 and Q. Fig. 11 compares the BT curves predicted by the deactivation kinetic model with experimental BT curves which indicates the parity with the Yoon–Nelson model.

Comparison of packed bed models

The R^2 values (~1) (Fig. 7) suggest the fitting of the BDST model for packed bed adsorption of MCPA on RHA. The results predicted by the BDST model inform that the length of MTZ is increased after 50 % BT. Among the other considered packed bed models, the values of deviations (MPSD and Є) indicate the aptness of the Bohart–Adams model for certain experiments only. On the other hand, the Thomas model is appropriate for experiments performed at lower operating values of C_0, Q, and Z. The least values of MPSD and Є clearly suggest the best fitting of Yoon–Nelson and deactivation kinetic models for complete saturation of column for all experiments. Therefore, in addition to conventional packed

Table 2 Comparison of adsorption capacity of different adsorbents for MCPA

Adsorbent	Capacity (mg/g)	Surface area (m^2/g)	Capacity (mg/m^2)	Reference
Filtrasorb-400 (GAC, F-400)	0.72	800	0.0009	(Cho et al. 2006)
Carbon black	37.1	137	0.271	(Nyazi et al. 2005)
Activated carbon	94.3	1225	0.077	(Pérez et al. 2012)
Activated carbon	94.1	1201	0.078	
Norit 0.8	133.61	1150	0.116	(Gimeno et al. 2003)
Aquacarb 207C	117.65	1150	0.102	
Aquacarb 208A	106.167	1250	0.085	
Aquacarb 208EA	105.26	1250	0.084	
Mg–Al–Cl–LDH	100	44	2.27	(Inacio et al. 2001)
Mg–Al–CO_3–LDH	16	83	0.192	
Mg–Al–CO_3–water/ethylene glycol–LDH	70	135	0.519	
Mg–Al–CO_3–water/acetone–LDH	36	95	0.379	
Activated spent bleaching earth	16.05	207	0.077	(Mahramanlioglu et al. 2003)
Activated spent bleaching earth	3.009[a]	207	0.015[a]	
Polymer resin	56.71[a]	1300	0.044[a]	(Vergili and Barlas 2009)
RHA	1.681	33.61	0.050	Present study
RHA	2.480[a]	33.61	0.073[a]	Present study

[a] Packed bed capacity

bed models, the deactivation kinetic model can be proposed for solid–liquid adsorption.

Comparison of adsorption capacities of different adsorbents

In Table 2, the adsorption capacity of various adsorbents reported in literature for MCPA removal is compared with the present adsorbent. However, it can be observed that the batch adsorption capacity (mg/g) of RHA is ~2.3 times greater than that of granular-activated carbon (GAC, Filtrasorb F-400). Besides, the batch adsorption capacity (mg/m^2) based on the surface area is ~55.55-fold higher for RHA than for GAC. Additionally, the RHA batch capacity (mg/m^2) is equivalent to that of few adsorbents such as activated carbon, aquacarb 208A, aquacarb 208EA, and activated spent bleaching earth. The packed bed capacity (mg/m^2) of RHA is greater than that of activated spent bleaching earth and polymer resin. Though the adsorption quantity (mg/g) of RHA is less, the advantage of this adsorbent is low cost, and this shows that it is still competitive for other adsorbents.

Conclusions

Adsorption capacity of RHA is greater than GAC and is equivalent with some of the adsorbents previously reported for MCPA removal. Adsorption kinetics obeys pseudo-second order and Elovich models suggesting the heterogeneous surface of RHA. The fitting of Langmuir isotherm infers the favorable adsorption in the temperature range of 303–328 K. The feasibility and spontaneity of adsorption are indicated by negative values of ΔG whereas the exothermic adsorption is indicated by negative value of ΔH. Bigger particles of RHA have higher BET surface area together with smaller silica to carbon ratio; therefore, the removal of MCPA is more on bigger particles than on smaller particles. The adsorption capacity of RHA in packed bed study is higher than in batch, indicating the effect of continuous contact between RHA and MCPA. The MTZ in packed bed adsorption does not move with constant velocity resulting in inconstant bed utilization. The application of packed bed models demonstrates the aptness of deactivation kinetic, Yoon–Nelson, and BDST models. Therefore, along with conventional packed bed models, deactivation kinetic model is recommended for solid–liquid adsorption.

Acknowledgement Authors are thankful to the Science and Engineering Research Board (SERB), India, for providing research grant (SB/S3/CE/077/2013) to undertake the work. Sophisticated characterization facilities provided by IBM, Nagpur, and CSMCRI, Bhavnagar (India), are acknowledged.

References

Ahmaruzzaman M, Gupta VK (2011) Rice husk and its ash as low-cost adsorbents in water and wastewater treatment. Ind Eng Chem Res 50:13589–13613

Akhtar M, Hasany SM, Bhanger MI et al (2007) Low cost sorbents for the removal of methyl parathion pesticide from aqueous solutions. Chemosphere 66:1829–1838

Aksu Z, Gönen F (2004) Biosorption of phenol by immobilized activated sludge in a continuous packed bed: prediction of breakthrough curves. Process Biochem 39:599–613

Arivazhagan M, Meenakshi R (2011) Quantum chemical studies on structure of 1-3-dibromo-5-chlorobenzene. Spectrochimi Acta A 82:316–326

Aziz ASA, Manaf LA, Man HC et al (2014) Column dynamic studies and breakthrough curve analysis for Cd(II) and Cu(II) ions adsorption onto palm oil boiler mill fly ash (POFA). Environ Sci Pollut Res 21: 7996–8005

Bruna F, Celis R, Pavlovic I et al (2009) Layered double hydroxides as adsorbents and carriers of the herbicide (4-chloro-2-methylphenoxy) acetic acid (MCPA): systems Mg–Al, Mg–Fe and Mg–Al–Fe. J Hazard Mater 168:1476–1481

Cabrera A, Cox L, Spokas K et al (2011) Comparative sorption and leaching study of the herbicides fluometuron and 4-chloro-2-methylphenoxyacetic acid (MCPA) in a soil amended with biochars and other sorbents. J Agric Food Chem 59:12550–12560

Cardoso LP, Valim JB (2006) Study of acids herbicides removal by calcined Mg—Al—CO_3—LDH. J Phys Chem Solids 67:987–993

Cho SY, Park SS, Kim SJ et al (2006) Adsorption and desorption characteristics of 2-methyl-4-chlorophenoxyacetic acid onto activated carbon. Korean J Chem Eng 23:638–644

Deokar SK, Mandavgane SA (2015a) Estimation of packed-bed parameters and prediction of breakthrough curves for adsorptive removal of 2,4-dichlorophenoxyacetic acid using rice husk ash. J Environ Chem Eng 3:1827–1836

Deokar SK, Mandavgane SA (2015b) Rice husk ash for fast removal of 2, 4-dichlorophenoxyacetic acid from aqueous solution. Adsorpt Sci Technol 33:429–440

Deokar SK, Mandavgane SA, Kulkarni BD (2016) Behaviour of biomass multicomponent ashes as adsorbents. Curr Sci 110:180–186

Dutta R, Nagarjuna TV, Mandavgane SA et al (2014) Ultrafast removal of cationic dye using agrowaste-derived mesoporous adsorbent. Ind Eng Chem Res 53:18558–18567

FAO (2014): Food and Agriculture Organization of the United Nations: Statistics Division, http://faostat3.fao.org/browse/Q/*/E

Gimeno O, Plucinski P, Kolaczkowski ST (2003) Removal of the herbicide MCPA by commercial activated carbons: equilibrium, kinetics, and reversibility. Ind Eng Chem Res 42:1076–1086

Han R, Wang Y, Zhao X et al (2009) Adsorption of methylene blue by phoenix tree leaf powder in a fixed-bed column: experiments and prediction of breakthrough curves. Desalination 245:284–297

Hiller E, Tatarková V, Šimonovicová A et al (2012) Sorption, desorption, and degradation of (4-chloro-2-methylphenoxy) acetic acid in representative soils of the Danubian Lowland, Slovakia. Chemosphere 87:437–444

Hermosin MC, Cornejo J (1993) Binding mechanism of 2,4-dichlorophenoxyacetic acid by organo-clays. J Environ Qual 22:325–331

Hong YS, Zhang ZF, Cai ZP et al (2014) Deactivation kinetics model of H_2S removal over mesoporous LaFeO3/MCM-41 sorbent during hot coal gas desulfurization. Energy Fuels 28:6012–6018

IARC (1983) Monographs on evaluation of the carcinogenic risk of chemicals to humans. http://monographs.iarc.fr/ENG/Monographs/vol1-42/mono30.pdf Accessed on 10/02/2016

Iglesias A, López R, Gondar D et al (2010) Adsorption of MCPA on goethite and humic acid-coated goethite. Chemosphere 78:1403–1408

Ignatowicz K (2009) Selection of sorbent for removing pesticides during water treatment. J Hazard Mater 169:953–957

Inacio J, Gueho CT, Forano C et al (2001) Adsorption of MCPA pesticide by MgAl-layered double hydroxides. Appl Clay Sci 18:255–264

Jain R, Sharma P, Sikarwar S (2013) Kinetics and isotherm analysis of Tropaeoline ooo adsorption onto unsaturated polyester resin (UPR): a non-carbon adsorbent. Environ Sci Pollut Res 20:1493–1502

Kim M, Hyun S (2014) Effect of surface coordination on 2,4-D sorption by kaolinite from methanol/water mixture. Chemosphere 103:329–335

Mahramanlioglu M, Kizilcikli I, Biçer IO et al (2003) Removal of MCPA from aqueous solutions by acid-activated spent bleaching earth. J Environ Sci Health B 38:813–827

Mane VS, Mall ID, Srivastava VC (2007) Kinetic and equilibrium isotherm studies for the adsorptive removal of Brilliant Green dye from aqueous solution by rice husk ash. J Environ Manag 84:390–400

Marczewska AD, Blachnio M, Marczewski AW et al (2010) Adsorption of selected herbicides from aqueous solutions on activated carbon. J Therm Anal Calorim 101:785–794

Nawaz S, Bhatti HN, Bokhari TH et al (2014) Removal of Novacron Golden Yellow dye from aqueous solutions by low-cost agricultural waste: batch and fixed bed study. Chem Eco 30:52–65

Nethaji S, Sivasamy A, Kumar RV (2013) Preparation of char from lotus seed biomass and the exploration of its dye removal capacity through batch and column adsorption studies. Environ Sci Pollut Res 20:3670–3678

Nyazi K, Bacaoui A, Yaacoubi A et al (2005) Influence of carbon black surface chemistry on the adsorption of model herbicides from aqueous solution. Carbon 43:2215–2234

Pérez RO, Daiem MMA, Utrilla JR et al (2012) Modeling adsorption rate of organic micropollutants present in landfill leachates onto granular activated carbon. J Colloid Interface Sci 385:174–182

Pavlovic I, Barriga C, Hermosın MC (2005) Adsorption of acidic pesticides 2,4-D, Clopyralid and Picloram on calcined hydrotalcite. Appl Clay Sci 30:125–133

Pavia DL, Lampman GM, Kriz GS et al (2008) Introduction to spectroscopy, 4th edn. Cengage Learning, USA

Preetha B, Viruthagiri T (2007) Batch and continuous biosorption of chromium(VI) by Rhizopus arrhizus. Sep Purif Technol 57:126–133

Singh N (2009) Adsorption of herbicides on coal fly ash from aqueous solutions. J Hazard Mater 168:233–237

Srivastava VC, Mall ID, Mishra IM et al (2006) Characterization of mesoporous rice husk ash (RHA) and adsorption kinetics of metal ions from aqueous solution onto RHA. J Hazard Mater B 134:257–267

Srivastava VC, Prasad B, Mishra IM et al (2008) Prediction of breakthrough curves for sorptive removal of phenol by bagasse fly ash packed bed. Ind Eng Chem Res 47:1603–1613

Sotelo J, Ovejero G, Rodríguez A et al (2012) Removal of atenolol and isoproturon in aqueous solutions by adsorption in a fixed bed column. Ind Eng Chem Res 51:5045–5055

Vergili I, Barlas H (2009) Removal of 2,4-D, MCPA and metalaxyl from water using Lewatit VP OC 1163 as sorbent. Desalination 249: 1107–1114

Wu Y, Wen Y, Zhou J et al (2013) Comparative and competitive adsorption of Cr(VI), As(III), and Ni(II) onot coconut charcoal. Environ Sci Pollut Res 20:2210–2219